How to cite: *Angew. Chem. Int. Ed.* **2021**, *60*, 1396–1402
International Edition: doi.org/10.1002/anie.202012059
German Edition: doi.org/10.1002/ange.202012059

Nanoparticles

Nanoscale Anatomy of Iron-Silica Self-Organized Membranes: Implications for Prebiotic Chemistry

*Electra Kotopoulou, Miguel Lopez-Haro, Jose Juan Calvino Gamez, and Juan Manuel García-Ruiz**

Abstract: *Iron-silica self-organized membranes, so-called chemical gardens, behave as fuel cells and catalyze the formation of amino/carboxylic acids and RNA nucleobases from organics that were available on early Earth. Despite their relevance for prebiotic chemistry, little is known about their structure and mineralogy at the nanoscale. Studied here are focused ion beam milled sections of iron-silica membranes, grown from synthetic and natural, alkaline, serpentinization-derived fluids thought to be widespread on early Earth. Electron microscopy shows they comprise amorphous silica and iron nanoparticles of large surface areas and inter/intraparticle porosities. Their construction resembles that of a heterogeneous catalyst, but they can also exhibit a bilayer structure. Surface-area measurements suggest that membranes grown from natural waters have even higher catalytic potential. Considering their geochemically plausible precipitation in the early hydrothermal systems where abiotic organics were produced, iron-silica membranes might have assisted the generation and organization of the first biologically relevant organics.*

Introduction

Two of the most critical steps in the emergence of life on Earth were concentration and oligomerization of the biologically relevant organic molecules. But, the information available about water bodies/primitive oceans on Hadean-early Archean Earth strongly suggests that concentrations of the abiotic building blocks (e.g. amides, lipids, amino acids, etc.) were too dilute for significant oligomerization to occur. To solve this conundrum, adsorption on mineral surfaces has been put forward as a plausible mechanism for the significant concentration of the first organic molecules.[1–8] In this context, multiple studies examined the role of mineral surfaces in the chemical polymerization reactions that might have taken place at early Earth, and in the formation of a proto-cellular membrane by allowing amphiphilic molecules, such as fatty acids, to interact with clays, silica, pyrite, iron-oxides, iron-sulfides etc., assisting the formation of a vesicle.[2,9–14] Based on these, and other works it is now generally accepted that mineral-mediated membranes may have provided a geochemical pathway to the transition from inorganic chemistry to biology.

Among all mineral-mediated pathways that have been explored so far, those related to chemical gardens, that is, inorganic, self-organized, metal/sulfide/silica(te) membranes, hold a special place. Self-organization of metal-silica membranes takes place spontaneously when an alkaline, silicate-rich solution reacts with a concentrated metal source (e.g. soluble Me-salt particle or Me-salt solution), due to a reaction-diffusion controlled precipitation process.[15,16] This leads to the formation of a diaphragm membrane with compartmentalized spaces, separating two very distinct chemical environments in terms of pH and ions concentrations. It has been shown that these drastic differences across the membrane generate electrochemical potential and electrical current, able to endure for several hours/days (as long as the system remains far from equilibrium), thus, presenting battery-like properties.[17,18]

Several studies have paralleled chemical garden formation to hydrothermal chimneys.[19–23] Indeed, similar proton and ion gradients may occur across some hydrothermal chimneys, such as those of the Strytan field in Iceland.[24] Yet, mineral precipitation in hydrothermal chimneys commonly occurs due to mixing of the hydrothermal fluids with seawater/meteoric water and pressure/temperature decrease, contrary to the chemical garden membranes precipitation. In the latter, the cations directly react with silicate (or other anions) and hydroxide ions to yield metal-silica(te) hydrates. Nonetheless, these mineral membranes are thought to have functioned as electron/proton conductors and redox catalysts at the early Earth hydrothermal vents, and the alkaline silica-rich, Hadean environments.[6,21,22,25] These settings have been proposed as the niches for the emergence of metabolism.[21,26]

Although a wide variety of synthetic and natural Me-membranes can be produced (e.g., Co^{2+}-/Ni^{2+}-/Ca^{2+}-/Zn^{2+}-/La^{2+}-/Cu^{2+}-/Mn^{2+}-/Mg^{2+}-/Cr^{3+}-salts)[27] those made with $Fe^{2+/3+}$ soluble particles/solutions are by far the most relevant

[*] E. Kotopoulou, Prof. Dr. J. M. García-Ruiz
Instituto Andaluz de Ciencias de la Tierra, Consejo Superior de Investigaciones Científicas- Universidad de Granada
Avda. de las Palmeras 4, 18100 Granada (Spain)
E-mail: juanmanuelgarcia@csic.es
Dr. M. Lopez-Haro, Prof. Dr. J. J. Calvino Gamez
Departamento de Ciencia de los Materiales e Ingeniería Metalúrgica y Química Inorgánica, Facultad de Ciencias, Universidad de Cadiz
Campus Rio San Pedro, Puerto Real, 11510 Cádiz (Spain)
Supporting information and the ORCID identification number(s) for the author(s) of this article can be found under: https://doi.org/10.1002/anie.202012059.

© 2020 The Authors. Angewandte Chemie International Edition published by Wiley-VCH GmbH. This is an open access article under the terms of the Creative Commons Attribution Non-Commercial NoDerivs License, which permits use and distribution in any medium, provided the original work is properly cited, the use is non-commercial and no modifications or adaptations are made.

for early Earth geochemistry and prebiotic chemistry. Iron is the fourth most abundant element in Earth's crust that has been readily available in early Earth (in the reduced form), being a primary component of the early oceans, sediments and hydrothermal precipitates.[28–30] The role of ferrous iron in prebiotic chemistry was recently highlighted by[31] that demonstrated that by mixing it with pyruvate and glyoxylate (two products of abiotic CO_2 reduction) they can make nine of the eleven intermediates of the biological Krebs cycle, including all five universal metabolic precursors, supporting the theory for a geochemical origin of the metabolism. With respect to the metal-silica membranes, those made with iron-salts/-salt solutions have been found to show the highest battery-like performance, generating more than 550 mV enduring for several hours.[17,18a] Moreover, it was demonstrated that iron membranes can catalyze the condensation of formamide (CH_3NO), a critical intermediate product in Miller-type reactions thought to be widespread in early Earth, yielding the four nucleobases of RNA, three amino acids and several carboxylic acids in a single experiment at 80 °C[7] and the formation of amino acids in presence of pyruvate ($CH_3COCO_2^-$).[25] Adding to these, iron-silica membranes are capable of providing ultraviolet (UV) radiation shielding to the newly forming molecules[32] which is a critical property considering the higher flux of UV radiation in early Earth.[33]

Last but not least, understanding inorganic filamentous iron-silica membranes can be relevant for the distinction of abiotic from biotic signatures in the rock record, due to their morphological and chemical resemblance to iron filaments found in cherts and silica-rich hydrothermal precipitates.[6,34–36]

The geochemical plausibility of the precipitation of these membranes in natural environments was investigated by a recent study which demonstrated that iron-silica membranes can form from natural solutions, by replacing the model silicate media with alkaline, silica-rich spring water (Ney, CA, USA).[27d] This water of pH 12 containing more than 4 gL^{-1} of silica, is discharging from a serpentinization setting and links the laboratory synthesis of the iron-silica membranes to a geological environment relevant for early Earth.[6,27d,37]

Yet, to fully understand the remarkable catalytic behavior of the iron-silica filamentous membrane and their putative role in prebiotic chemical reactions and primitive life detection studies, it is paramount to have a detailed characterization of their internal anatomy, that is, mineral chemistry and structure. Recent studies reported that these membranes are composed of a mixture of amorphous metal-silicate/silica and crystalline iron hydroxides/oxides.[7,18b,38–43] However, we still lack information about the precise mineral phases that make up these nanocomposite membranes and how these phases are distributed/organized at the nanoscale. Moreover, there is very little information about the composition of the natural iron-silica membranes and if the extraordinary properties of the synthetic membranes can be extended to the natural ones as well.

To address this knowledge gap we have used a series of transmission electron microscopy techniques for the study of the internal structure and mineral chemistry of iron-silica membranes, made with both model and natural solutions (Ney water, CA, USA). We show that the membranes are composed of iron nanophases of akaganeite, goethite and magnetite and amorphous silica, the properties and structure of which can be directly related to the catalytic potential of the membranes. Also, we demonstrate that these inorganic self-organized membranes can have a bilayer structure. Provided that geochemical environments considered to be plausible for the formation of iron-silica membranes on early Earth were also likely to contain significant amounts of abiotic organics, our results give grounds to the hypothesis that these membranes could have played a key role in the adsorption, condensation and organization of simple organic molecules on early Earth, while providing electron/proton conductors and redox catalysts to drive prebiotic reactions.

Results

We performed a scanning transmission electron microscopy and spectroscopy study of FIB-milled sections obtained from model iron-silica membranes, that is, made with soluble Fe^{II}-chloride pellet and sodium silicate solution, and natural ones, that is, those made using natural water from the Ney spring, California in place of the silicate solution (see Supporting Information for details). In the case of the model membranes, microscopic observation of the FIB sections showed that the membrane wall is composed of two layers separated by a sharp boundary (Figure 1 A–E).

Elemental mapping of Si, O, Fe, Cl and Na in the model membrane revealed that the external layer is composed of silicon dioxide and the internal one of iron-(oxy)hydroxides/

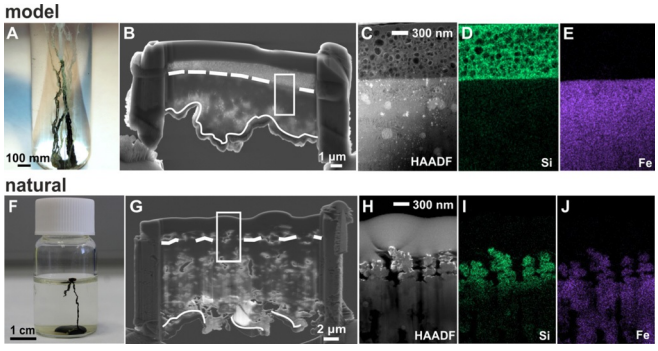

Figure 1. FIB-milled sections of the Fe^{II}-silica tubular membranes made with the model sodium silicate solution and the natural Ney water. A) Fe^{II}-silica tubular membrane made with the model silicate sol. B) SEM image of the FIB-milled section of the model membrane, where the layers are shown. The white lines separate the exterior silica layers from the interior iron-rich layer. C–E) HAADF image and Si, Fe elemental maps of the model membrane. Notice the sharp boundary between the exterior silica and interior iron-rich layer. Silica reappears after the iron-rich part. F) Fe^{II}-silica tubular membrane made with the natural water. G) SEM image of the FIB-milled section of the natural membrane, where the silica-rich and iron-rich layers are shown. The white lines separate the exterior silica layer from the interior iron-rich layer. H–J) HAADF image and Si and Fe elemental maps of the natural membrane.

 © 2020 The Authors. Angewandte Chemie International Edition published by Wiley-VCH GmbH

-oxides. A few sodium chloride crystals, byproducts of the reaction between the sodium silicate and the iron chloride, crystalized on the membrane upon drying (Figure 1C and Figure S2 in the Supporting Information). Furthermore, both elemental maps, and line sections, crossing both layers, demonstrate that there is no transition zone between the two layers. Hence, no Fe-silicates are formed in the walls of the membranes.

Si $L_{2,3}$-edge ELNES characterization (in the energy-loss range 90–200 eV) of the outer layer of the membrane confirmed that the external side is composed of amorphous silica. As indicated in Figure S1 the spectra show the typicaL L-edges of silica at 106 eV, 113.5 eV and at 130 eV with respect to reference sample.[44,45] The inner layer of the membrane wall, in close contact with the outer layer is composed of compactly arranged 5–10 nm sized Fe-(oxy)-hydroxide particles. The HR-HAADF study showed that these particles correspond to akaganeite (β-FeOOH), containing up to 2% of Cl (Figure 2A,B). Experimental and simulation data show very high correlation and allow identification of different planes of the akaganeite crystals. Figure 2B shows an akaganeite nanocrystal viewed along the [010] zone axis, where two series of nanotunnels can be identified, with diameters of 7.5 Å and 3.5 Å, respectively. Moving inwards from the outer wall to the internal part there is a transition to larger crystals in the range of 50–150 nm (Figure 2A–C). As shown in Figure 2D we identified rhombohedral goethite (α-FeOOH) and rhombohedral magnetite (Fe_3O_4).

The natural membranes are less rigid and exhibit higher porosity compared to the model membranes. Likewise, the external silica part, that is, the outer tube wall, is amorphous as confirmed by Si $L_{2;3}$-edge ELNES (Figure S1), but is thinner than the model membrane (< 1 μm). XEDS mapping indicated a correlation between Si, O and Fe (Figure 1H–J). However, this spatial correlation does not correspond to an iron-silicate zone, rather to iron nanoparticles over the amorphous silica support. The internal tube wall is composed of goethite and magnetite platelets with a thickness of ≈5–10 nm and an average length of ≈100–200 nm (Figure 2D,E).

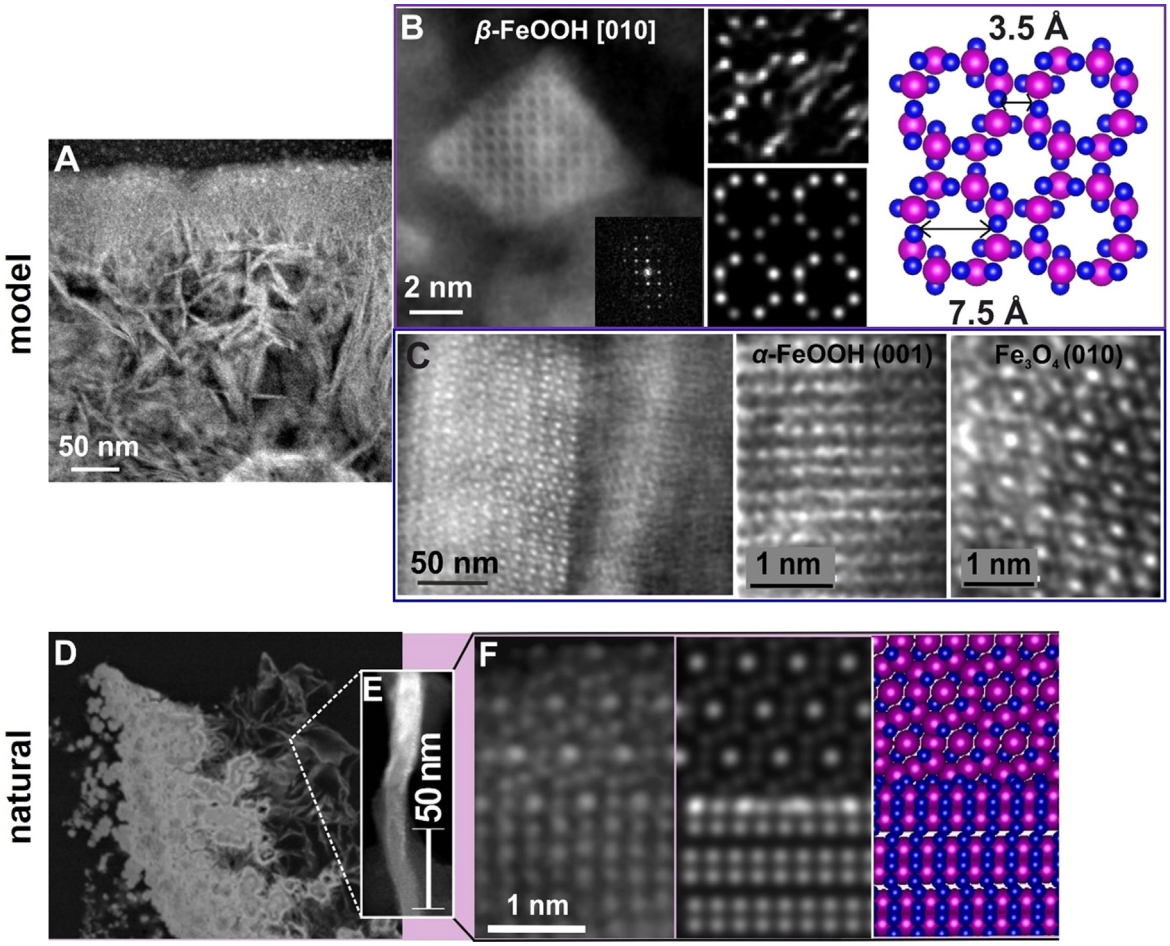

Figure 2. HR-HAADF study and atomic simulations of the internal Fe-rich part of the model and natural membranes. A) Medium magnification HAADF image of the Fe-rich layer of the model membrane, where compact size crystals develop to elongated larger crystals forming platelets. B) HR-HAADF image of the compact zone and simulation data showing the akaganeite phase, viewed from the [010] direction. Note the size of the nanochannels in the akaganeite structure (Cl atoms are not shown here). C) HR-HAADF images of the platelets composed of magnetite and goethite. D) Medium magnification STEM image of the horizontal section of the Fe-Ney tubular membrane showing the membrane layers. E) Close up of the internal layer of the Fe-platelets. F) HR-HAADF image, simulation and structural model of (E) depicting the topotactic transformation of rhombohedral magnetite to rhombohedral goethite.

 © 2020 The Authors. Angewandte Chemie International Edition published by Wiley-VCH GmbH

Following the tubular membrane growth and allowing the system to reach equilibrium ($\approx$70 h),[18b] evaporation of the outer solution and/or CO_2 atm diffusion in the sol, provoked silica supersaturation, inducing silica re-precipitation. Therefore, since the tubular membranes are hollow, silica reappears after the iron-oxyhydroxide layer, as shown in the study of focused ion beam (FIB) milled sections (Figure 1B,G, Figure S2C and Figure 3). This feature, previously overlooked, owing to tubes extraction soon after their formation, gives rise to a bilayer membrane where the external silica layers enclose the iron nanoparticles (Figure 3). Continuing silica precipitation ultimately encases the tubes in the silica gel, as shown in Figure S2A.

To estimate the specific surface area (SSA) of the model and natural membranes that is directly related to their catalytic performance we used the Brunauer-Emmet-Teller (BET) (N_2) method (according to [46]). Both membranes exhibit high active surface area. As inferred from the results of the TEM study and as measured by BET analysis, the natural membrane has higher specific surface area, 140 $m^2 g^{-1}$, than that of the model membrane, 113 $m^2 g^{-1}$. This can be attributed to the higher intra-particulate porosity of the natural membrane with respect to the model that exhibited a more compact structure. However, we should note that BET analysis tends to underestimate the SSA in case of particle aggregation, such as in the case of the iron platelets formed in both membranes, due to certain inaccessibility of nonpolar gases (e.g., N_2) to particle boundaries within aggregates.[47]

Discussion

The nanoscale study performed here revealed the anatomy of the iron-silica filamentous membranes that are made of amorphous silica layers enclosing an internal layer of nanosized iron-(oxy)hydroxides. In contrast to previous studies that reported the presence of a Me-silicate zone,[15,17] our results show no iron-silicates. This seems to be a result of limitations in the analytical techniques previously used, coupled with the presence of amorphous silica that hinders the identification of the rest of the phases. We should note that in another ex-situ study of iron-silica gardens (using a ferrous chloride seed, similar to here) they did not detect an external silica layer at all,[18b] but they attributed this either to an isolation artifact or to the tube density with respect to the size of the silicate species. The sharp transition between the two layers shown here (Figure 1), is a result of the mechanism of the membrane growth that compartmentalizes two sides of distinct physicochemical conditions. As demonstrated elsewhere ([18b]) during the tube growth, ferrous iron cations are trying to penetrate the tube wall from the inside, they oxidize and precipitate as iron-oxyhydroxides once in contact with the, high pH, outer silicate solution. Conversely, silicate ions, following the reverse path, polymerize as soon as they experience the low pH of the Fe-rich solution and amorphous silica precipitates on the outer wall of the membrane.

As for the case of the natural membranes, despite growing them from a natural solution (Ney spring water; see Table S1), they exhibit a similar make-up to that of the model ones. Both synthetic and natural membranes show external amorphous silica layers enclosing an internal iron-oxyhydroxides/-oxides layer. With respect to this internal layer, goethite and magnetite were present in both membranes, likely resulting from an akaganeite precursor ([48–52]). Yet, akaganeite, was only detected in model membranes, in proximity to the silica layer. The absence of akaganeite from the natural membranes can be related to the lower silica concentration of the Ney water, used for their growth (see Experimental Methods, SI and Table S1). Previous studies have shown that in alkaline media, silicate is known to retard the transformation of akaganeite to goethite by stabilization against dissolution and interference in goethite nucleation. This is owed to absorption of the silicic acid on the Fe-OH sites of the akaganeite that commonly replace the Cl in the outer surface of the structure ([53,54]). Nonetheless, the absence of akaganeite from the natural membranes does not

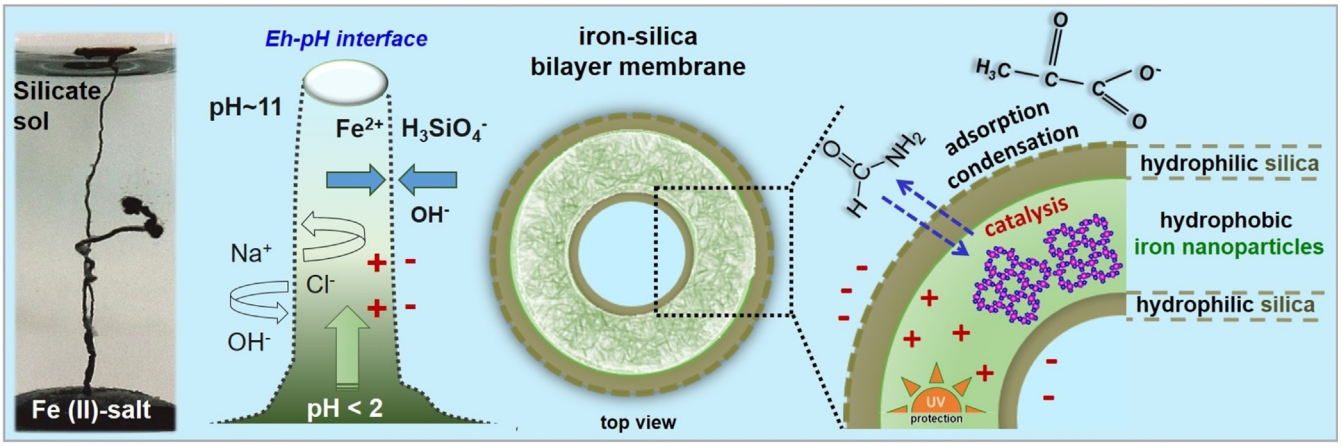

Figure 3. Inorganic iron-silica membranes behave as fuel cells and are capable of adsorbing and condensing organic molecules and catalyzing the formation of amino acids, nucleobases and carboxylic acids, while providing UV radiation shielding. These membranes, that could have precipitated in the early Earth hydrothermal environments (among other settings), may have provided a template for the concentration and organization of the first organic molecules in a bilayer membrane.

 © 2020 The Authors. Angewandte Chemie International Edition published by Wiley-VCH GmbH

seem to affect their catalytic potential since membranes grown from natural water show higher micro- and nanoporosity (STEM study) and higher specific surface area, as shown from the BET measurements. These findings suggest that membranes precipitating from natural solutions are potentially better catalysts than the model ones.

Previous work with iron tubes proposed that the electrochemical voltage generated across the membrane, owing to the drastic redox and pH differences of the membrane layers, might provide catalytic properties to the chemical gardens. Here we argue that, in addition, the structure and nanomineralogy of the iron-silica membranes control the catalytic function of the membranes. The nanoscale study of the FIB-milled sections of both model and natural membranes demonstrated that the composition of the membrane is similar to that of a heterogeneous catalyst, that is, iron-(oxy)hydroxides dispersed onto a silica amorphous support. In fact, silica is considered an ideal substrate for nanoparticle dispersion in heterogeneous catalysis as it hinders nanoparticle aggregation while increasing the active surface area of the particles.[40,55–59] Moreover, it has been demonstrated that at alkaline pH the surface charge density of silica is negative and the dissociation of the terminal silanol groups provides an interface where thin films of organics or metals can be adsorbed and concentrated, thus, enhancing condensation reactions.[55,60–62]

At the same time, the iron nanoparticles that constitute the internal wall of the membrane have received great attention for their catalytic and magnetic performance in a range of applications. Particularly, akaganeite, magnetite and goethite are used in phenol hydroxylation, the Fenton reaction, Michael additions and isomerization, in the manufacturing of electric and magnetic materials, water treatment, labeling and magnetic separation of biological materials, directed drug delivery and more.[63] Our study showed that the iron particles of the model and natural iron-silica membranes exhibit very small particle size (< 10 nm), large surface areas, high pore volumes and both micro-interparticle and nano-intraparticle porosity; hence exhibiting high catalytic potential. Particularly interesting for the role of iron-silica membranes in prebiotic chemistry is the fact that iron nanoparticles catalyze the Fischer–Tropsch (FT) synthesis of abiotic organic molecules, which has been shown to take place in submarine hydrothermal vents.[64–66] Adding to this, a recent study demonstrated that during FT-reactions iron nanoparticles synthesized on a mesoporous silica support, similar to the iron-silica membranes, exhibit a strong selectivity for the production of CH_4 in presence of H_2.[57,58,67]

Overall, the self-organized iron-silica membranes bring together two distinct layers with different physicochemical and structural properties. The chemical and mineralogical compartmentalization of the iron-silica membranes make each layer contribute in a different way in the overall catalytic performance of the membrane. With respect to the yielding of amino acids, carboxylic acids and nucleobases molecules by formamide condensation onto the membranes, we hypothesize that the outer silica layer assists formamide or pyruvate adsorption and condensation, while the simultaneous precipitation of at least two different iron-oxyhydroxides in the internal wall of the membrane may be responsible for the variety of the organic molecules generated in the internal environment.[25,32,68]

Our results show that under certain, geochemically plausible conditions (i.e. evaporation, and/or temperature increase and/or CO_2 diffusion in the solution) the iron-silica membranes exhibit a bilayer structure where the external silica hydrophilic layers encapsulate the hydrophobic iron-oxyhydroxides (Figure 3 and Figure S2). This feature is particularly interesting considering that amphiphilic molecules that could be products of FT reactions in hydrothermal systems[69,70] show high affinity for both silica and iron-oxyhydroxides.[55,59] Furthermore, as shown here (Figure S2A) continuing silica precipitation will finally encase the membranes in the silica gel. Taking into account their geochemically plausible formation in natural environments, this feature would facilitate their preservation in the rock record.[71]

Although there is no rock record from the Hadean period, it is now generally accepted that low temperature ($< 250\,°C$) hydrothermal serpentinization reactions of ultramafic rocks, like those occurring at the "Lost City" vents in the Atlantic Ocean, may generate alkaline fluids with high concentrations of H_2 and CH_4 and were widespread on early Earth.[6,66,72,73] In these type of settings, reaction of the silicate anions with aqueous ferrous iron, or iron nanoparticles, originating from high temperature water–rock interactions, or, from runoff/aeolian erosion of subaerial ultramafic rocks would induce the precipitation of iron-silica membranes.[27d,74,75] Then, the iron-silica membranes would react with abiotic organics, like formamide, pyruvate, or CH_4, generated from FT reactions, as a consequence of hydrothermal serpentinization and other mineral redox processes.[7,64,66,70a,73] In this context, organic molecules could be adsorbed into the outer silica layer of the iron-silica membranes, enhancing condensation reactions and would be brought in contact with the iron catalysts of the inner layer. Provided that tubular membranes would be formed, silica re-precipitation (provoked by evaporation, CO_2atm diffusion and/or temperature increase) and following bilayer formation might have provided an inorganic, self-organizing, template for the effective oligomerization of the produced organics and the organization in an organic bilayer membrane.

Conclusion

We have studied the nanoscale anatomy of FIB-milled sections of iron-silica membranes, also known as chemical gardens, grown from both synthetic and natural solutions, unveiling their structure, mineralogy and catalytic potential. Our results show that iron-silica self-organized membranes are built of different nanosized iron-(oxy)hydroxide phases over an amorphous silica support, similar to the structure of a silica-based heterogeneous catalyst. Based on our TEM and BET results we can conclude that mineral membranes grown from natural spring water, analogous to the early Earth aqueous settings, may hold even higher catalytic potential for prebiotic reactions than the synthetic ones. This finding

 © 2020 The Authors. Angewandte Chemie International Edition published by Wiley-VCH GmbH

supports the geochemical plausibility of the role of membranes in catalyzing the building blocks of life from simple reactions, such as, formamide or pyruvate condensation, or, FT-type organics produced in hydrothermal settings. At the same time, these membranes could have provided an inorganic template for the concentration and organization of the organic molecules (once they have formed) in a bilayer membrane, under a self-organizing mechanism. Since ferrous iron, silica saturated waters and abiotic organics were thought to be widespread in early Earth and Earth-like planets (e.g., Mars), iron-silica self-organization might have played a universal role in the geochemical origin of life.[6,30,70a,76–79]

Supporting Information: Experimental Procedures. Figure S1: Si $L_{2,3}$-edge ELNES of the external side of the model and natural membranes matching the α-SiO_2 reference sample (reference after Batson, 1991 EELS Database). Figure S2: STEM -EDX maps and lines crossing the membranes layers. Table S1: Chemical analysis of the Ney water.

Acknowledgements

We acknowledge Dr. Guerra-Tschuschke for assistance with the SEM-EDX study from the Centro de Instrumentación Científica (CIC) of the University of Granada, Spain and Francisca Espinosa Perez from the Laboratorio de Estudios Cristalograficos, of the Instituto Andaluz de Ciencias de la Tierra (IACT), Granada, Spain for helping with the silica garden experiments. Concepción Hernández Castillo from the Centro de Instrumentación Científica (CIC) of the University of Granada, Spain, is acknowledged for technical assistance with the microtome sectioning of the membranes, and Stephan Borensztajn from the Institut de Physique du Globe de Paris (IPGP), Paris, France for the FIB-milling of the tubules. Valérie Magnin from the Plateforme Géochimie-Minéralogie of the Institut des Sciences de la Terre (ISTerre), Grenoble, France assisted with the BET measurements. MLH and JJCG acknowledge financial support from MINECO/FEDER (Projects MAT2017-87579-R and MAT2016-81118-P) and Junta de Andalucía (FQM334). HR-STEM analysis were performed using the facilities at the DME-UCA node of the ICTS ELECMI. This work received funding from the European Research Council under the Programme (FP7/2007–2013)/ERC Grant Agreement 340863 (Prometheus).

Conflict of interest

The authors declare no conflict of interest.

Keywords: heterogeneous catalysis · iron · membranes · nanoparticles · prebiotic chemistry

[1] D. W. Deamer, J. P. Dworkin, S. A. Sandford, M. P. Bernstein, L. J. Allamandola, *Astrobiology* **2002**, *2*, 371 – 382.
[2] M. M. Hanczyc, S. M. Fujikawa, J. W. Szostak, *Science* **2003**, *302*, 618 – 622.
[3] P. Dalai, H. Kaddour, N. Sahai, *Elements* **2016**, *12*, 401 – 406.
[4] R. M. Hazen, D. A. Sverjensky, *Cold Spring Harbor Perspect. Biol.* **2010**, *2*, a002162.
[5] R. J. Gillams, T. Z. Jia, *Life* **2018**, *8*, 10.
[6] J. M. García-Ruiz, M. van Zuilen, W. Bach, *Phys. Life Rev.* **2020**, https://doi.org/10.1016/j.plrev.2020.07.004.
[7] B. M. Bizzarri, L. Botta, M. I. Perez-Valverde, R. Saladino, E. Di Mauro, J. M. García-Ruiz, *Chemistry* **2018**, *24*, 8126 – 8132.
[8] F. Westall, K. Hickman-Lewis, N. Hinman, P. Gautret, K. A. Campbell, J. G. Bréhéret, F. Foucher, A. Hubert, S. Sorieul, A. V. Dass, T. P. Kee, T. Georgelin, A. Brack, *Astrobiology* **2018**, *18*, 259 – 293.
[9] M. M. Hanczyc, S. S. Mansy, J. W. Szostak, *Origins Life Evol. Biospheres* **2007**, *37*, 67 – 82.
[10] N. Sahai, H. Kaddour, P. Dalai, Z. Wang, G. Bass, M. Gao, *Sci. Rep.* **2017**, *7*, 43418.
[11] P. A. Monnard, D. W. Deamer, *Anat. Rec.* **2002**, *268*, 196 – 207.
[12] W. Martin, M. J. Russell, *Philos. Trans. R. Soc. London Ser. B* **2003**, *358*, 59 – 85.
[13] J. P. Ferris, G. Ertem, *Origins Life Evol. Biospheres* **1992**, *22*, 369 – 381.
[14] a) H. J. Cleaves II, et al., *Chem. Soc. Rev.* **2012**, *41*, 5502 – 5525; b) I. B. Gorrell, T. W. Henderson, K. Albdeery, P. M. Savage, T. P. Kee, *Life* **2017**, *7*, 45.
[15] J. H. E. Cartwright, J. M. García-Ruiz, M. L. Novella, F. Otálora, *J. Colloid Interface Sci.* **2002**, *256*, 351 – 359.
[16] S. Thouvenel-Romans, O. Steinbock, *J. Am. Chem. Soc.* **2003**, *125*, 4338 – 4341.
[17] F. Glaab, M. Kellermeier, W. Kunz, E. Morallon, J. M. García-Ruiz, *Angew. Chem. Int. Ed.* **2012**, *51*, 4317 – 4321; *Angew. Chem.* **2012**, *124*, 4393 – 4397.
[18] a) L. M. Barge, Y. Abedian, M. J. Russell, I. J. Doloboff, J. H. Cartwright, R. D. Kidd, I. Kanik, *Angew. Chem. Int. Ed.* **2015**, *54*, 8184 – 8187; *Angew. Chem.* **2015**, *127*, 8302 – 8305; b) F. Glaab, J. Rieder, J. M. García-Ruiz, W. Kunz, M. Kellermeier, *Phys. Chem. Chem. Phys.* **2016**, *18*, 24850 – 24858.
[19] S. E. McGlynn, I. Kanik, M. J. Russell, *Philos. Trans. R. Soc. London Ser. A* **2012**, *370*, 3007 – 3022.
[20] L. M. Barge, I. J. Doloboff, M. J. Russell, D. VanderVelde, L. M. White, G. D. Stucky, M. M. Baum, J. Zeytounian, R. Kidd, I. Kanik, *Geochim. Cosmochim. Acta* **2014**, *128*, 1 – 12.
[21] W. Martin, J. Baross, D. Kelley, M. J. Russell, *Nat. Rev. Microbiol.* **2008**, *6*, 805 – 814.
[22] M. J. Russell, R. M. Daniel, A. J. Hall, J. A. Sherringham, *J. Mol. Evol.* **1994**, *39*, 231 – 243.
[23] F. M. Möller, F. Kriegel, M. Kieß, V. Sojo, D. Braun, *Angew. Chem. Int. Ed.* **2017**, *56*, 2340 – 2344; *Angew. Chem.* **2017**, *129*, 2380 – 2384.
[24] R. Price, E. S. Boyd, T. M. Hoehler, L. M. Wehrmann, E. Bogason, H. Þ. Valtýsson, J. Örlygsson, B. Gautason, J. P. Amend, *Geology* **2017**, *45*, 1135 – 1138.
[25] L. M. Barge, E. Flores, M. M. Baum, D. G. VanderVelde, M. J. Russell, *Proc. Natl. Acad. Sci. USA* **2019**, *116*, 4828 – 4833.
[26] M. Preiner, K. Igarashi, K. B. Muchowska, M. Yu, S. J. Varma, K. Kleinermanns, M. K. Nobu, Y. Kamagata, H. Tüysüz, J. Moran, W. F. Martin, *Nat. Ecol. Evol.* **2020**, *4*, 534 – 542.
[27] a) L. M. Barge, S. S. Cardoso, J. H. Cartwright, G. J. Cooper, L. Cronin, A. De Wit, I. J. Doloboff, B. Escribano, R. E. Goldstein, F. Haudin, D. E. Jones, A. L. Mackay, J. Maselko, J. J. Pagano, J. Pantaleone, M. J. Russell, C. I. Sainz-Diaz, O. Steinbock, D. A. Stone, Y. Tanimoto, N. L. Thomas, *Chem. Rev.* **2015**, *115*, 8652 – 8703; b) J. H. E. Cartwright, B. Escribano, C. I. Sainz-Díaz, *Langmuir* **2011**, *27*, 3286 – 3293; c) E. Nakouzi, O. Steinbock, *Sci. Adv.* **2016**, *2*, e1601144; d) J. M. García-Ruiz, E. Nakouzi, E. Kotopoulou, L. Tamborrino, O. Steinbock, *Sci. Adv.* **2017**, *3*, e1602285; e) H. Satoh, K. Tsukamoto, J. M. García-Ruiz, *Eur. J. Mineral.* **2014**, *26*, 415 – 426; f) M. Kellermeier, F. Glaab, E. Melero-García, J. M. García-Ruiz in *Methods in Enzymology*,

 © 2020 The Authors. Angewandte Chemie International Edition published by Wiley-VCH GmbH

Vol. 532 (Ed.: J. J. De Yoreo), Academic Press, New York, **2013**, pp. 225 – 256.
[28] R. L. Rudnick, D. M. Fountain, *Rev. Geophys.* **1995**, *33*, 267 – 309.
[29] B. Rasmussen, B. Krapež, J. R. Muhling, A. Suvorova, *Geology* **2015**, *43*, 303 – 306.
[30] I. Halevy, M. Alesker, E. M. Schuster, R. Popovitz-Biro, Y. Feldman, *Nat. Geosci.* **2017**, *10*, 135 – 139.
[31] K. B. Muchowska, S. J. Varma, J. Moran, *Nature* **2019**, *569*, 104 – 107.
[32] R. Saladino, G. Botta, B. M. Bizzarri, E. Di Mauro, J. M. García-Ruiz, *Biochemistry* **2016**, *55*, 2806 – 2811.
[33] C. S. Cockell, *Planet. Space Sci.* **2000**, *48*, 203 – 214.
[34] J. M. García-Ruiz, S. T. Hyde, A. M. Carnerup, A. G. Christy, M. J. Van Kranendonk, N. J. Welham, *Science* **2003**, *302*, 1194.
[35] S. McMahon, *Proc. R. Soc. London Ser. B* **2019**, *286*, 20192410.
[36] K. C. Johannessen, N. McLoughlin, P. E. Vullum, I. H. Thorseth, *Geobiology* **2020**, *18*, 31 – 53.
[37] a) I. Barnes, J. B. Rapp, J. R. O'Nefl, *Contrib. Mineral. Petrol.* **1972**, *35*, 263 – 276; b) T. Boschetti, L. Toscani, P. Iacumin, E. Selmo, *Aquat. Geochem.* **2017**, *23*, 299 – 313; c) G. E. J. G. Blank, V. Stamenković, A. R. Rowe, I. Kohl, S. Li, E. D. Young, *Astrobiology Science Conference 2017*, **2017**, p. 3608.
[38] D. Balköse, F. Özkan, U. Köktürk, S. Ulutan, S. Ülkü, G. Nişli, *J. Sol-Gel Sci. Technol.* **2002**, *23*, 253 – 263.
[39] K. Parmar, A. K. Pramanik, N. R. Bandyopadhya, S. Bhattacharjee, *Mater. Res. Bull.* **2010**, *45*, 1283 – 1287.
[40] R. Makki, O. Steinbock, *J. Am. Chem. Soc.* **2012**, *134*, 15519 – 15527.
[41] L. M. Barge, I. J. Doloboff, L. M. White, G. D. Stucky, M. J. Russell, I. Kanik, *Langmuir* **2012**, *28*, 3714 – 3721.
[42] L. M. Barge, S. S. Cardoso, J. H. Cartwright, I. J. Doloboff, E. Flores, E. Macias-Sanchez, C. I. Sainz-Diaz, P. Sobron, *Proc. R. Soc. London Ser. A* **2016**, *472*, 20160466.
[43] F. Glaab, J. Rieder, R. Klein, D. Choquesillo-Lazarte, E. Melero-Garcia, J. M. García-Ruiz, W. Kunz, M. Kellermeier, *ChemPhysChem* **2017**, *18*, 338 – 345.
[44] P. E. Batson, *Phys. Rev. B* **1991**, *44*, 5556 – 5561.
[45] J. B. Neaton, D. A. Muller, N. W. Ashcroft, *Phys. Rev. Lett.* **2000**, *85*, 1298 – 1301.
[46] L. Clausen, I. Fabricius, *J. Colloid Interface Sci.* **2000**, *227*, 7 – 15.
[47] H. Y. Jeong, J. H. Lee, K. F. Hayes, *Geochim. Cosmochim. Acta* **2008**, *72*, 493 – 505.
[48] M. A. Blesa, M. Mijalchik, M. Villegas, G. Rigotti, *React. Solids* **1986**, *2*, 85 – 94.
[49] H. Tanaka, R. Mishima, N. Hatanaka, T. Ishikawa, T. Nakayama, *Corros. Sci.* **2014**, *78*, 384 – 387.
[50] C. Rémazeilles, P. Refait, *Corros. Sci.* **2007**, *49*, 844 – 857.
[51] Y. T. He, S. J. Traina, *Clay Miner.* **2007**, *42*, 13 – 19.
[52] P. Refait, J. M. R. Génin, *Corros. Sci.* **1997**, *39*, 539 – 553.
[53] R. M. Cornell, R. Giovanoli, *Clays Clay Miner.* **1990**, *38*, 469 – 476.
[54] G. Naren, A. Miyazaki, M. Matsuo, S. Bai, K. Yonesu, Y. Okaue, T. Yokoyama, *Chin. J. Geochem.* **2013**, *32*, 27 – 34.
[55] N. Kensuke, K. Iwaki, N. Kitano, A. Ohki, S. Maeda, *Polym. J.* **1996**, *28*, 911 – 915.
[56] Y. Li, W.-N. Wang, Z. Zhan, M.-H. Woo, C.-Y. Wu, P. Biswas, *Appl. Catal. B* **2010**, *100*, 386 – 392.
[57] T. Zhang, M. D. Amiridis, *Appl. Catal. A* **1998**, *167*, 161 – 172.
[58] H. Suo, S. Wang, C. Zhang, J. Xu, B. Wu, Y. Yang, H. Xiang, Y.-W. Li, *J. Catal.* **2012**, *286*, 111 – 123.
[59] A. Králík, M. Hansen, B. König, *RSC Adv.* **2016**, *6*, 5739 – 5744.
[60] S. K. Parida, S. Dash, S. Patel, B. K. Mishra, *Adv. Colloid Interface Sci.* **2006**, *121*, 77 – 110.
[61] M. Signorile, C. Salvini, L. Zamirri, F. Bonino, G. Martra, M. Sodupe, P. Ugliengo, *Life* **2018**, *8*, 42.
[62] Y. Wang, F. Caruso, *Chem. Commun.* **2004**, 1528 – 1529.
[63] D. L. Huber, *Small* **2005**, *1*, 482 – 501.
[64] T. M. McCollom, J. S. Seewald, *Chem. Rev.* **2007**, *107*, 382 – 401.
[65] D. I. Foustoukos, W. E. Seyfried, *Science* **2004**, *304*, 1002.
[66] G. Proskurowski, M. D. Lilley, J. S. Seewald, G. L. Früh-Green, E. J. Olson, J. E. Lupton, S. P. Sylva, D. S. Kelley, *Science* **2008**, *319*, 604.
[67] K. Jothimurugesan, J. J. Spivey, S. K. Gangwal, J. G. Goodwin in *Studies in Surface Science and Catalysis*, *Vol. 119* (Eds.: A. Parmaliana, D. Sanfilippo, F. Frusteri, A. Vaccari, F. Arena), Elsevier, Amsterdam, **1998**, pp. 215 – 220.
[68] B. Mattia Bizzarri, L. Botta, M. I. Perez-Valverde, R. Saladino, E. Di Mauro, J. M. García-Ruiz, *Chem. Eur. J.* **2018**, *24*, 8126 – 8132.
[69] T. M. McCollom, G. Ritter, B. R. T. Simoneit, *Origins Life Evol. Biospheres* **1999**, *29*, 153 – 166.
[70] a) B. Ménez, C. Pisapia, M. Andreani, F. Jamme, Q. P. Vanbellingen, A. Brunelle, L. Richard, P. Dumas, M. Réfrégiers, *Nature* **2018**, *564*, 59 – 63; b) A. I. Rushdi, B. R. T. Simoneit, *Origins Life Evol. Biospheres* **2001**, *31*, 103 – 118.
[71] E. Kotopoulou, *Mineral self-organization in extreme geochemical environments: implications for prebiotic chemistry and life detection*, Doctoral dissertation, University of Granada, Spain, **2020**.
[72] N. H. Sleep, A. Meibom, T. Fridriksson, R. G. Coleman, D. K. Bird, *Proc. Natl. Acad. Sci. USA* **2004**, *101*, 12818 – 12823.
[73] F. Klein, N. G. Grozeva, J. S. Seewald, *Proc. Natl. Acad. Sci. USA* **2019**, *116*, 17666.
[74] O. J. Rouxel, A. Bekker, K. J. Edwards, *Science* **2005**, *307*, 1088.
[75] J. Rouillard, J. M. García-Ruiz, J. Gong, M. A. van Zuilen, *Geobiology* **2018**, *16*, 279 – 296.
[76] R. Siever, *Geochim. Cosmochim. Acta* **1992**, *56*, 3265 – 3272.
[77] N. J. Tosca, S. Guggenheim, P. K. Pufahl, *Geol. Soc. Am. Bull.* **2016**, *128*, 511 – 530.
[78] W. W. Fischer, A. H. Knoll, *Geol. Soc. Am. Bull.* **2009**, *121*, 222 – 235.
[79] L. M. Barge, *Nat. Commun.* **2018**, *9*, 5170.

Manuscript received: September 3, 2020
Accepted manuscript online: October 6, 2020
Version of record online: November 25, 2020

 © 2020 The Authors. Angewandte Chemie International Edition published by Wiley-VCH GmbH